STING-mediated degradation of IFI16 negatively regulates apoptosis by inhibiting p53 phosphorylation at serine 392

Dapei Li[1,2,*,‡], Lifen Xie[1,2,‡], Zigang Qiao[1,2], Sanyue Mai[3], Jingfei Zhu[1,2], Fan Zhang[1,2], Shengchuan Chen[2,4], Liang Li[1,2,4], Fangrong Shen[5], Yanghua Qin[6], Haiping Yao[1,2], Sudan He[1,2], and Feng Ma[1,2,4,*]

From the [1]Center for Systems Medicine, Institute of Basic Medical Sciences, Chinese Academy of Medical Sciences & Peking Union Medical College, Beijing, China; [2]Suzhou Institute of Systems Medicine, Suzhou, China; [3]Department of Laboratory Medicine, 988 Central Hospital of People's Liberation Army, Zhengzhou, China; [4]Department of Hepatopancreatobiliary Surgery, The First Affiliated Hospital of Wenzhou Medical University, Wenzhou, China; [5]Department of Obstetrics and Gynecology, The First Affiliated Hospital of Soochow University, Suzhou, China; [6]Department of Laboratory Diagnosis, Changhai Hospital of the Second Military Medical University, Shanghai, China

Edited by Eric Fearon

Interferon-γ–inducible factor 16 (IFI16) triggers stimulator of interferon (IFN) genes (STING)–dependent type I IFN production during host antiviral immunity and facilitates p53-dependent apoptosis during suppressing tumorigenesis. We have previously reported that STING-mediated IFI16 degradation negatively regulates type I IFN production. However, it is unknown whether STING also suppresses IFI16/p53-dependent apoptosis *via* degradation of IFI16. Here, our results from flow cytometry apoptosis detection and immunoblot assays show that IFI16 and nutlin-3, a p53 pathway activator, synergistically induce apoptosis in U2OS and A549 cells. Protein kinase R–triggered phosphorylation of p53 at serine 392 is critical for the IFI16-p53–dependent apoptosis. However, overexpression of STING suppresses p53 serine 392 phosphorylation, p53 transcriptional activity, expression of p53 target genes, and p53-dependent mitochondrial depolarization and apoptosis. In summary, our current study demonstrates that STING-mediated IFI16 degradation negatively regulates IFI16-mediated p53-dependent apoptosis in osteosarcoma and non–small cell lung cancer cells, which suggests a protumorigenic role for STING in certain cancer types because of its potent ability to degrade upstream IFI16.

Interferon (IFN)-γ–inducible factor 16 (IFI16) is a member of the IFN-inducible PYHIN protein family of nuclear proteins and considered as an important DNA sensor in recognizing pathogenic DNA (1). It contains a PYRIN domain (PYD) at the N-terminus and two conserved hematopoietic expression, IFN-inducible, and nuclear location (HIN) domains (HIN-A and HIN-B) at the C-terminus (2, 3). The PYD of IFI16 mediates homotypic and heterotypic protein–protein interaction, which is responsible for signaling transduction (4). IFI16 interacts with the adaptor molecule apoptosis-associated speck like protein containing a caspase recruitment domain *via* the

PYD–PYD interactions to form a functional inflammasome during Kaposi sarcoma–associated herpesvirus infection (5, 6). IFI16 also interacts with stimulator of IFN genes (STING) to activate the downstream TANK-binding kinase 1–IFN regulatory factory 3–IFN-β signaling axis *via* its PYD (7). The C-terminal HIN-A and HIN-B domains have been implicated in DNA binding and mediating protein–protein interaction for transcriptional regulation (8). For example, HIN-A domain binds to the C-terminal region of p53, whereas the HIN-B domain binds to the core DNA-binding region of p53, which synergistically contributes to the effect of IFI16 on p53–DNA complex formation and transcriptional activation (9).

In addition to the roles in DNA sensing and activating antiviral immunity, IFI16 negatively regulates tumorigenesis by interacting with p53 or inducing transcription of p53 (8–10). As a DNA damage amplifier, IFI16 interacts with p53, promotes p53 phosphorylation at serine 15 (Ser15), and thus participates in the accumulation and activation of p53 caused by DNA damage, which ultimately promotes p53-dependent apoptosis (8, 10). Besides the Ser15 residue, the highly conserved residue, serine 392 (Ser392) (Ser389 in mice), is also a major phosphorylation site of p53. Ser392 phosphorylation is a common and integral event during p53 activation under diverse stimuli such as UV or the murine double minute 2 (MDM2)-p53 antagonist nutlin-3 treatment (11–13). Several protein kinases including casein kinase 2, p38 mitogen-activated protein kinase, and protein kinase R (PKR) have been shown to be responsible for p53 Ser392 phosphorylation (14–16). However, it is still unknown whether IFI16, the p53 positive regulator, facilitates these protein kinase–mediated Ser392 phosphorylation of p53 and p53-dependent apoptosis.

STING-dependent signaling pathway plays important roles in antitumor immunity and tumor immunotherapy. Endogenous STING agonist cyclic guanosine monophosphate–adenosine monophosphate from tumor cells triggers a STING-mediated IFN response in nontumor cells to activate the antitumor response of natural killer cells (17). Synthetic small-molecule amidobenzimidazole-based compounds effectively bind and activate STING. Amidobenzimidazole

---

derivatives elicit strong antitumor activity, with complete and lasting regression of tumors (18). Other synthetic STING agonists such as 5,6-dimethylxanthenone-4-acetic acid and cyclic di-AMP have been demonstrated to strongly induce IFN-β in both murine macrophages and primary human cells, decrease tumor sizes on the xenografted murine melanoma, colon, and breast models, and induce antitumor immunological memory following tumor regression (19). However, as a potent type I IFN (IFN-I) inducer, activated STING also promotes tumor initiation, growth, and metastasis in a stage-specific manner. In prostate cancer, cytosolic dsDNA accumulation coupled with STING signaling increases from hyperplasia to stage II and then decreases in stage III (20). STING activation is associated with increased tumor growth in the noninflammatory Lewis lung carcinoma mouse model (21). In breast cancer and lung cancer, cyclic guanosine monophosphate–adenosine monophosphate can be transferred from tumor cells to astrocytes through gap junctions, which further activate STING, IFN-I, and NF-κB signaling in the astrocytes and thus promote tumor brain metastasis (22). Our previous study has shown that STING negatively controls IFI16 expression by degrading upstream excessive IFI16 during antiviral immunity (7). As IFI16 cooperates with p53 to inhibit tumorigenesis, it drives us to investigate whether STING-mediated degradation of upstream IFI16 also suppresses IFI16-p53–dependent apoptosis, and whether STING plays a protumor role independent of activating its downstream IFN-I and NF-κB signaling.

In this study, we have shown that IFI16 promotes p53-dependent apoptosis, the loss of mitochondrial membrane potential ($\Delta\Psi_m$), p53 Ser392 phosphorylation, p53 transcriptional activity, and expression of p53 target genes in human osteosarcoma and NSCLC cells. However, STING suppresses these IFI16-mediated antitumor effects by degrading upstream IFI16 protein. Herein, we have outlined an alternative pathway that STING plays a detrimental role in antitumor signaling in addition to be beneficial in antiviral immunity.

Results

Opposite effects of IFI16 and STING in the regulation of p53-dependent apoptosis

To determine whether IFI16 regulates p53-dependent apoptosis in osteosarcoma cells, we deleted *IFI16* gene in U2OS cells using the CRISPR/Cas9 technology. Nutlin-3, a p53–MDM2 antagonist and p53 pathway activator, promoted U2OS apoptosis in a dose-dependent manner (Fig. 1, *A* and *B*). However, knockout of IFI16 significantly abolished the induction of apoptosis by nutlin-3 (Fig. 1, *A* and *B*). Consistently, the cleavage of caspase 3, a critical executioner of apoptosis, was also undetectable in the *IFI16*$^{-/-}$ cells, whereas it was highly induced in the high-dose nutlin-3-treated *WT* cells (Fig. 1*C*), which suggests that IFI16 and nutlin-3 may synergistically induce and stabilize p53 to activate p53-dependent apoptosis. Next, we selected the *WT* and *IFI16*$^{-/-}$ single-cell clones to confirm the aforementioned phenotypes (Fig. S1A and Fig. 1*D*, *bottom panel*). IFN-γ treatment further facilitated

nutlin-3–induced apoptosis in the *WT* clones, whereas much fewer apoptotic cells were detected in the *IFI16*$^{-/-}$ clones than that in the *WT* clones (Fig. 1*D*, *upper panel*). IFI16 is an IFN-γ–inducible gene in multiple cell types (3, 23), and we found that overexpression of IFI16 also promoted nutlin-3–induced apoptosis in both U2OS and A549 cells, which is similar to the IFN-γ treatment (Fig. 1, *E* and *F*). The p53-specific inhibitor pifithrin-α abolished the apoptosis induced by nutlin-3 treatment and overexpression of IFI16 in A549 cells (Fig. 1*G*).

Interestingly, overexpression of STING, a downstream adaptor protein of IFI16 to induce IFN-I during DNA virus infection (1), significantly suppressed nutlin-3–induced apoptosis in U2OS cells (Fig. 1*H*). In addition, we checked the cell viability in the IFI16-overexpressed or STING-overexpressed cells. Overexpression of IFI16 inhibited cell viability in a dose-dependent manner (Fig. S1B), whereas overexpression of STING maintained cell viability in the A549 cells treated with a relative high concentration of nutlin-3, which induced apoptosis dramatically (Fig. S1C). Similar to the phenomenon observed in A549 cells, the opposite effects of IFI16 and STING in the regulation of cell viability were also shown in the U2OS cells treated with 40 μM nutlin-3 (Fig. S1D). Defective functional p53 signaling in the NCI-H1299 cells was reported previously (24, 25), and we found that overexpression of IFI16 and STING did not affect nutlin-3–induced apoptosis in the NCI-H1299 cells (Fig. 1, *I* and *J*).

Taken together, overexpression or induction of IFI16 facilitates p53-dependent apoptosis and inhibits cell viability, whereas overexpression of STING suppresses p53-dependent apoptosis and maintains cell viability during nutlin-3 treatment.

Opposite effects of IFI16 and STING in the regulation of $\Delta\Psi_m$

$\Delta\Psi_m$ is a key indicator of cell health or injury, and the loss of $\Delta\Psi_m$ usually leads to mitochondria-associated apoptosis. During the early stage of apoptosis, $\Delta\Psi_m$ decreases, and thus, the ratio of monomers to aggregates increases in the JC-1 assay (26). To verify whether the IFI16 or nutlin-3–induced apoptosis was resulted from $\Delta\Psi_m$ loss, we measured the $\Delta\Psi_m$ in A549 cells or U2OS cells treated with nutlin-3, showing that the $\Delta\Psi_m$ significantly decreased during nutlin-3 treatment at the dose, which is sufficient to induce the expression of cleaved caspase 3 and apoptosis (Fig. 2, *A*–*C*). Overexpression of IFI16 promoted the loss of $\Delta\Psi_m$ in cells treated with low-dose nutlin-3 (Fig. 2*B*). Consistently, less loss of $\Delta\Psi_m$ was observed in *IFI16*$^{-/-}$ U2OS cells than in the *WT* cells (Fig. 2*C*). Similar to the results from *IFI16*$^{-/-}$ cells, overexpression of STING also suppressed the loss of $\Delta\Psi_m$ in A549 cells treated with nutlin-3 at a concentration over 10 μM (Fig. 2*D*). Overexpression of IFI16 or STING did not affect the loss of $\Delta\Psi_m$ in p53 functional-defective NCI-H1299 cells (Fig. 2, *E* and *F*). The loss of $\Delta\Psi_m$ is frequently a decisive event of p53-dependent apoptosis (27). Therefore, these results suggest the opposite role of IFI16 and STING in the regulation of p53-mitochondrial pathway–associated apoptosis.
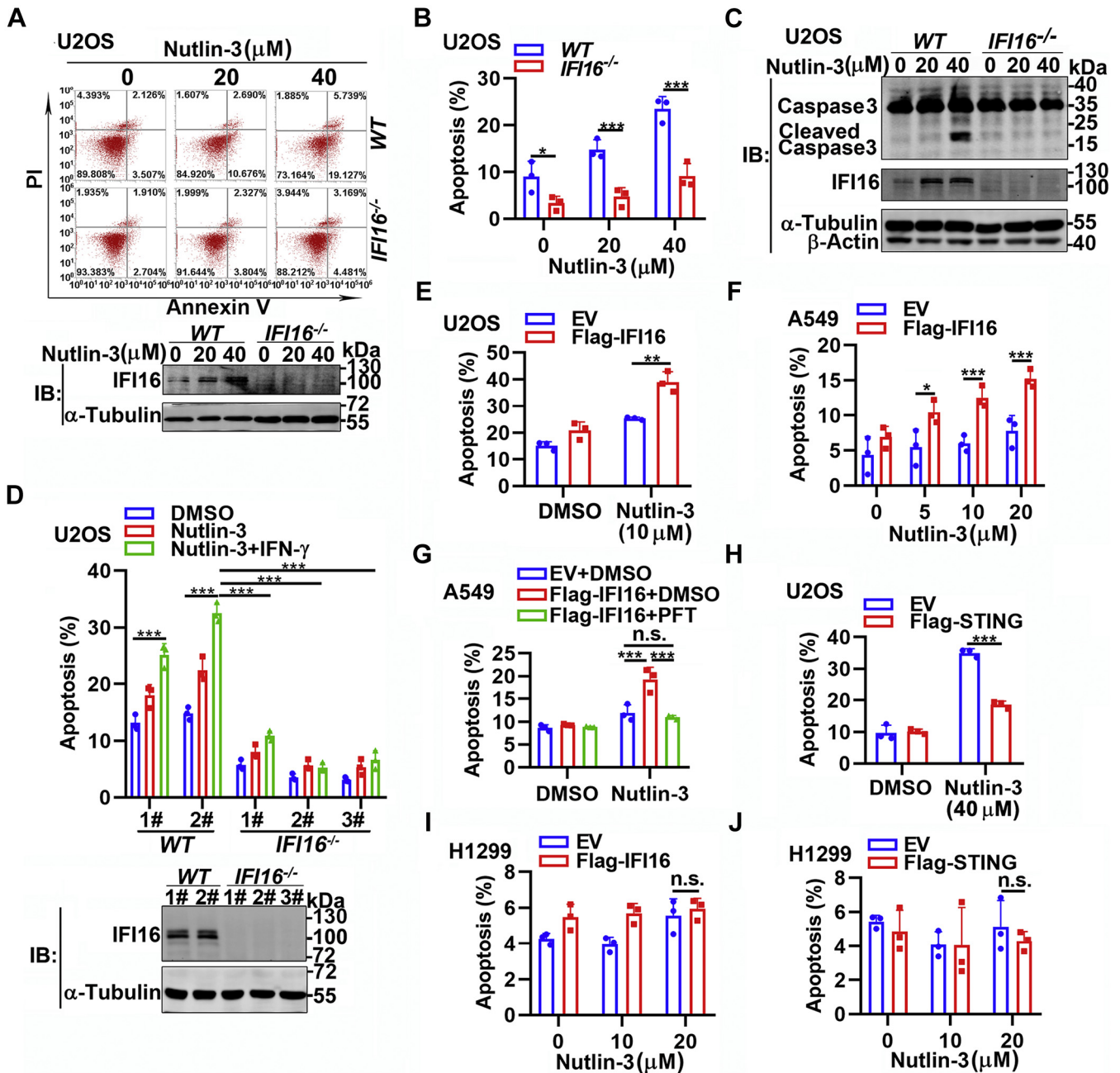
Figure 1. IFI16 and STING perform opposite effects in the regulation of p53-dependent apoptosis. *A* and *B*, *WT* and *IFI16*^{−/−} U2OS cells were treated with indicated concentration (0, 20, 40 μM) of nutlin-3 for 24 h, and the cells were harvested and stained with annexin V/PI for apoptosis analysis by flow cytometry. IFI16 protein levels were measured by IB, and α-Tubulin was shown as a loading control (*A*). Annexin V^{+} cells were considered as apoptotic cells, and the percentage was calculated (*B*). *C*, *WT* and *IFI16*^{−/−} U2OS cells were treated with indicated concentration (0, 20, 40 μM) of nutlin-3 for 24 h. The whole cell lysates were subjected to IB analysis with indicated antibodies for cleaved caspase 3 detection. *D*, clones of *WT* and *IFI16*^{−/−} U2OS were treated with DMSO, nutlin-3 (40 μM), and IFN-γ (20 ng/ml) for 18 h, and the cells were harvested and stained by annexin V/PI for apoptosis analysis. IFI16 protein levels were measured by IB, and α-Tubulin was shown as a loading control. *E* and *F*, empty vectors (EVs, 1 μg) or Flag-IFI16 (1 μg) vectors were transfected into U2OS or A549 cells (12-well plate), and the cells were treated with DMSO or nutlin-3 (*E*, 10 μM; *F*, 0, 5, 10, and 20 μM) for 24 h. The cells were harvested by trypsin digestion and stained by annexin V/PI for apoptosis analysis. *G*, EVs (1 μg) or Flag-IFI16 (1 μg) vectors transfected with A549 cells were administrated with nutlin-3 (20 μM) or/and pifithrin-α (PFT-α, 10 μM) for 24 h. The cells were harvested, and apoptotic cells were analyzed by flow cytometry. *H*, U2OS cells were transfected with EV (0.5 μg) or Flag-STING (0.5 μg) plasmids and treated with nutlin-3 (40 μM) for 24 h. The cells were harvested, and apoptotic cells were analyzed by flow cytometry. *I* and *J*, EV (*I*, 1 μg; *J*, 0.5 μg), Flag-IFI16 (1 μg), or Flag-STING (0.5 μg) vectors-transfected NCI-H1299 cells (12-well plate) were treated with nutlin-3 (0, 10, 20 μM) for 24 h. The cells were harvested by trypsin digestion and stained by annexin V/PI for apoptosis percentage analysis by flow cytometry. The experiment was repeated three times, and the data in *B* and *D*–*J* are expressed as mean ± SD (*$p < 0.05$, **$p < 0.01$, ***$p < 0.001$; unpaired Student's *t* test). DMSO, dimethyl sulfoxide; IB, immunoblotting; IFI16, interferon-γ–inducible factor 16; IFN-γ, interferon gamma; ns, not significant; PI, propidium iodide; STING, stimulator of interferon genes.
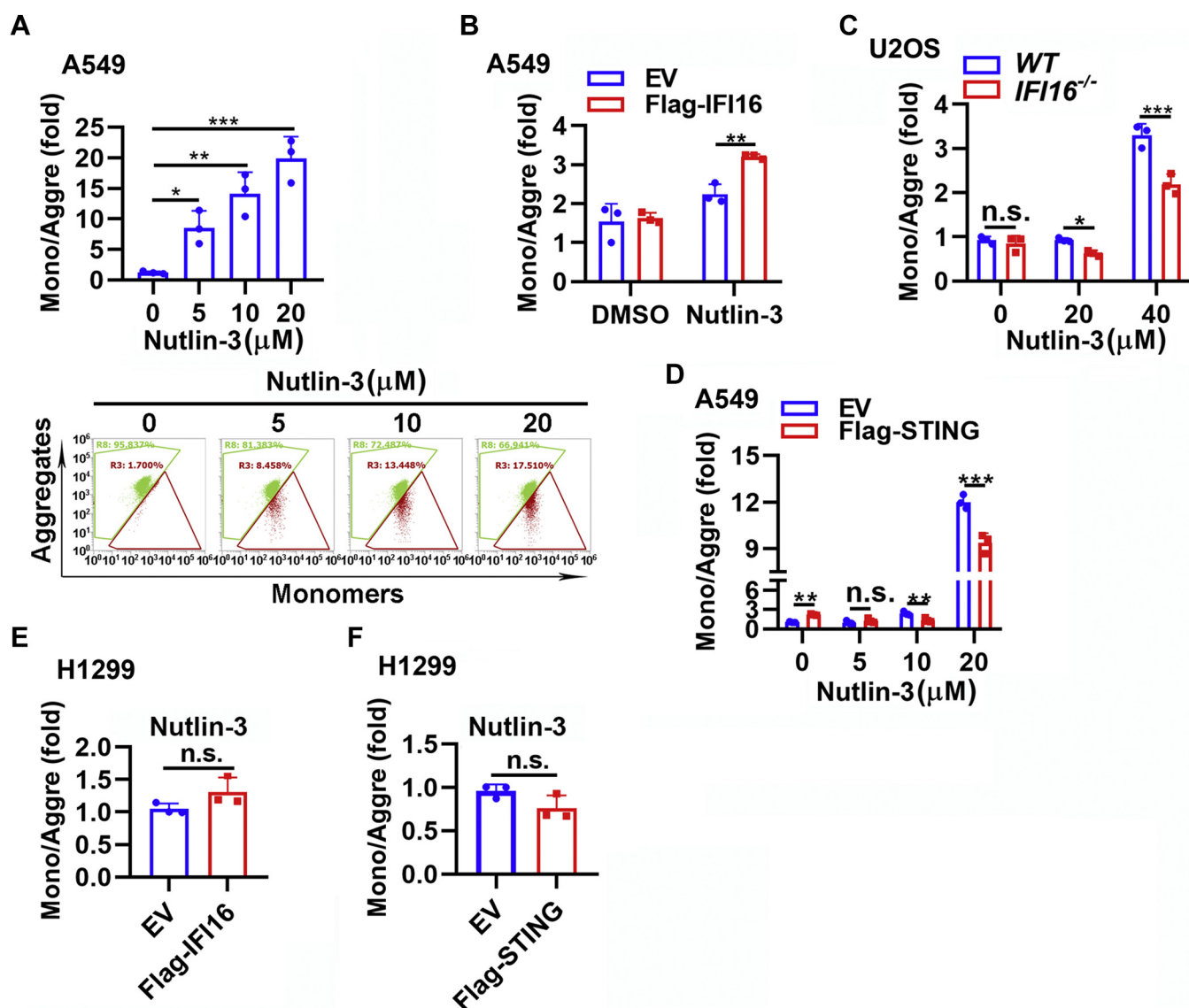
Figure 2. IFI16 and STING perform opposite effects in regulating the $\Delta\Psi_m$. *A*, A549 cells treated with the indicated concentration of nutlin-3 for 24 h were harvested by trypsin digestion and stained with JC-1 dye for $\Delta\Psi_m$ analysis by flow cytometry. *B* and *D*, A549 cells transfected with EV (*B*, 1 μg; *D*, 0.5 μg), Flag-IFI16 (1 μg), or Flag-STING (0.5 μg) vectors and treated with nutlin-3 (*B*, 5 μM; *D*, 0, 5, 10, and 20 μM) for 24 h were harvested and stained by JC-1 dye for $\Delta\Psi_m$ analysis. *C*, *WT* and *IFI16*$^{-/-}$ U2OS cells treated with nutlin-3 (0, 20, and 40 μM) for 24 h were harvested by trypsin digestion and stained by JC-1 dye for $\Delta\Psi_m$ analysis. *E* and *F*, EV (*E*, 1 μg; *F*, 0.5 μg), Flag-IFI16 (1 μg), or Flag-STING (0.5 μg) vector-transfected NCI-H1299 cells (12-well plate) were treated with nutlin-3 (20 μM) for 24 h. The cells were harvested by trypsin digestion and stained by JC-1 dye for $\Delta\Psi_m$ analysis. The experiments were repeated three times, and the data are expressed as mean ± SD (*$p < 0.05$, **$p < 0.01$, ***$p < 0.001$; unpaired Student's *t* test). EV, empty vector; IFI16, interferon-γ–inducible factor 16; ns, not significant; STING, stimulator of interferon genes.

Opposite effects of IFI16 and STING in the regulation of p53 transcriptional activity

To further investigate the roles of IFI16 and STING in the regulation of p53 signaling activation, we took advantage of p53-luc, a p53 luciferase reporter, to measure p53-mediated transcriptional activities quantitatively. Nutlin-3 treatment activated the p53 transcriptional activity in a dose-dependent manner in A549 cells (Fig. 3, *A* and *B*). Consistently, cisplatin (CDDP), another inducer of p53-dependent apoptosis (28), also significantly induced p53 transcriptional activity in U2OS cells (Fig. S2A). IFN-γ treatment further induced p53-luc activity in the A549 cells treated with nutlin-3 (Fig. 3B). Knockout of *IFI16* suppressed the p53-luc activity driven by nutlin-3 treatment in U2OS cells (Fig. 3C). Overexpression of

IFI16 induced p53-luc activity in the absence and presence of nutlin-3 (Fig. 3D), whereas overexpression of STING suppressed p53-luc activity (Fig. 3E). P53 functions as a transcription factor in the p53 regulatory network by targeting multiple genes (29–31). P53 target genes p53-upregulated modulator of apoptosis (*PUMA*), Bcl-2–associated X protein (*BAX*), and *P21* were significantly induced in the nutlin-3–treated cells (Fig. S2B). Knockout of IFI16 suppressed the induction of *PUMA* mRNA by nutlin-3 in the absence or presence of IFN-γ (Fig. 3F). Similarly, stable overexpression of STING also suppressed the induction of *PUMA* and *BAX*, both of which are critical in the mitochondrial apoptosis pathway, in the U2OS cells treated with nutlin-3 and IFN-γ (Fig. 3, *G* and *H*).
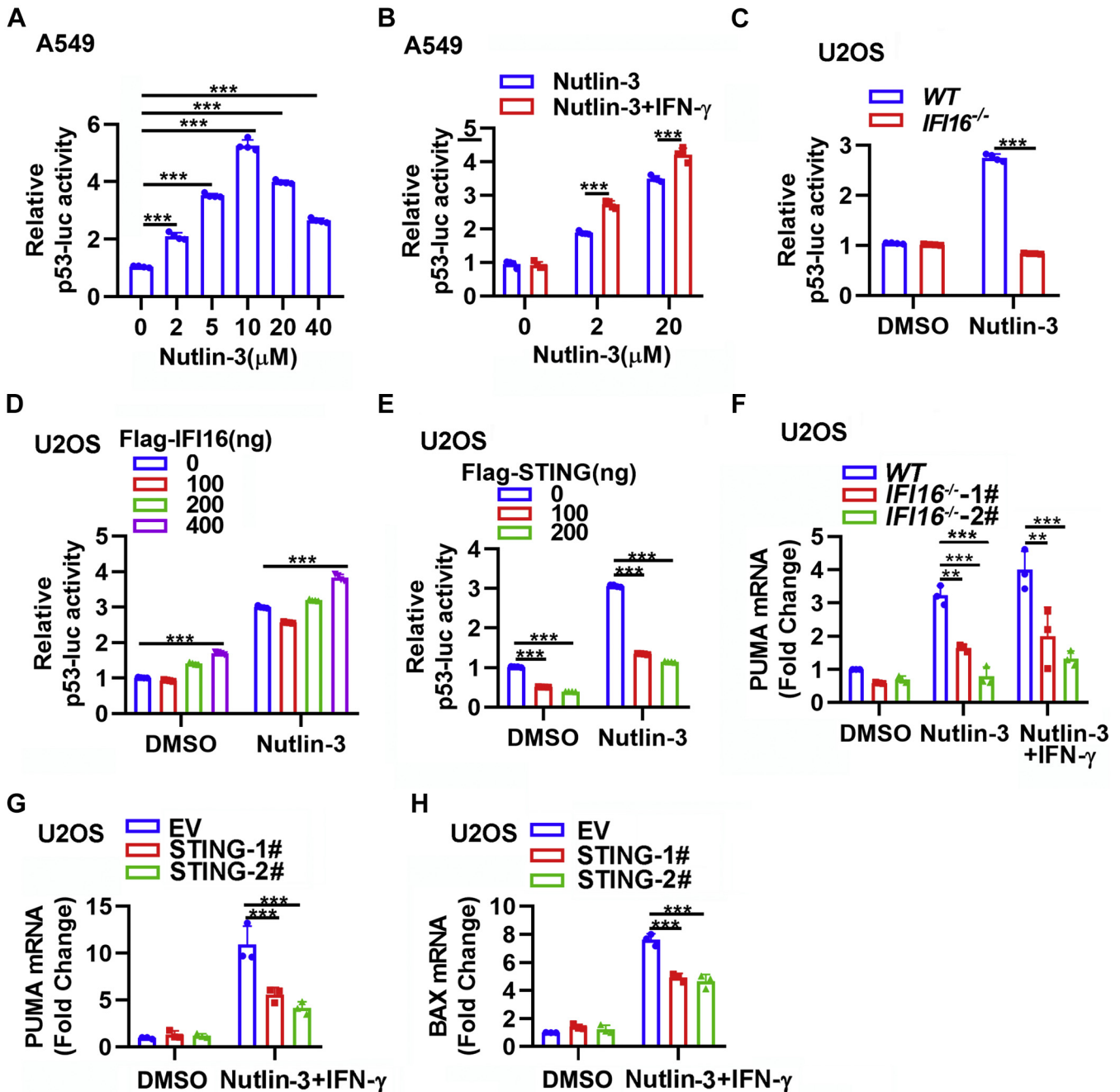
Figure 3. IFI16 and STING perform opposite effects in the regulation of p53 transcriptional activation. *A–C*, A549 (*A* and *B*), *WT*, and *IFI16$^{-/-}$* U2OS (*C*) cells in 24-well plates were transfected with a firefly p53-luc (p53-luciferase reporter, 150 ng), and these cells were treated with nutlin-3 and IFN-γ (*A*, 0, 2, 5, 10, and 20 μM; *B*, 0, 2, and 20 μM nutlin-3, 20 ng/ml IFN-γ; *C*, 5 μM nutlin-3) for 24 h. Relative firefly luciferase activity was quantified 32 h after transfection. *D* and *E*, U2OS cells in 24-well plates were cotransfected with p53-luc (150 ng) and the indicated amount of Flag-IFI16, Flag-STING–expressing plasmids. About 8 h after transfection, nutlin-3 (*D*, 10 μM; *E*, 20 μM) was added into the medium. Relative firefly luciferase activity was quantified 24 h later. *F–H*, *WT* and *IFI16$^{-/-}$* U2OS (*F*) or EV and STING stably overexpressed monoclonal cells (*G* and *H*) were treated with nutlin-3 (30 μM) and IFN-γ (*F*, 10 ng/ml; *G* and *H*, 20 ng/ml) for 24 h (*F*) or 18 h (*G* and *H*). The mRNA expression levels of *PUMA* and *BAX* were measured by RT-quantitative PCR. The experiment was repeated three times, and the data are expressed as mean ± SD (**$p < 0.01$, ***$p < 0.001$; unpaired Student's *t* test). *BAX*, Bcl-2–associated X protein; IFI16, interferon-γ–inducible factor 16; IFN-γ, interferon gamma; *PUMA*, p53 upregulated modulator of apoptosis; STING, stimulator of interferon genes.

In summary, we have found that IFI16 facilitates while STING suppresses the p53-dependent apoptosis, the loss of ΔΨ$_m$, p53 transcriptional activity, and the expression of p53 target genes in A549 and U2OS cells rather than in the NCI-H1299 cells, in which the functional p53 signaling is defective.

Ser392 phosphorylation of p53 during the activation of IFI16-p53 signaling

Post-translational modification of p53 by phosphorylation has been well proved to be an important mechanism for p53 stabilization and activation (32). To verify whether the robust apoptosis induced by high-dose nutlin-3 were resulting from

p53 phosphorylation, we checked most of the phosphorylation sites of p53 and found that Ser392-phosphorylated p53 was gradually induced in the U2OS cells treated with different concentrations of nutlin-3 (Fig. 4*A*). However, much less Ser392-phosphorylated p53 was detected in the *IFI16*$^{-/-}$ cells than that in WT cells (Fig. 4*A*). Overexpression of IFI16 facilitated Ser392 phosphorylation of p53 in U2OS, A549, and NCI-H460 cells treated with lower dose of nutlin-3. However, the Ser15 phosphorylation and total p53 expression were not induced consistently in all three cell lines (Fig. 4, *B* and *C* and Fig. S3*A*). We checked the protein levels of IFI16, p53, and STING in U2OS, A549, and NCI-H1299 cell lines. High expression of IFI16 and undetectable STING was in U2OS cells (Fig. S3*B*). A549 cells expressed the highest p53, medium IFI16, and STING among the three cell types (Fig. S3*B*). The higher STING, the lower IFI16, and p53 were detected in the aforementioned three cell types indicated a negative correlation between STING and IFI16-p53 signaling (Fig. S3*B*). Moreover, overexpression of STING suppressed the induction of IFI16 in these tumor cell lines, which finally restricted p53 accumulation (Fig. S3*C*). No endogenous Ser392-phosphorylated p53 was detected even in the nutlin-3–treated and IFI16-overexpressed NCI-H1299 cells, which might partially account for the functional defects in the NCI-H1299 cells (Fig. 4*D*).

Several kinases have been reported to be responsible for Ser392 phosphorylation of p53, such as p38 mitogen-activated protein kinase and the IFN-activated dsRNA-dependent protein kinase R (15, 16). We checked whether IFI16 affected p38- or PKR-mediated Ser392 phosphorylation of p53. Interaction analysis results showed that overexpression of IFI16 facilitated endogenous PKR-p53 binding but not p38-p53 binding, although IFI16 promoted both exogenous PKR–p53 and p38–p53 interaction (Fig. 4, *E* and *F* and Fig. S3, *D* and *E*). Overexpression of PKR triggered Ser392 phosphorylation of p53 in A549 cells (Fig. S3*F*). IFI16 colocalized with the PKR-Ser392–phosphorylated p53 complexes and facilitated PKR-mediated Ser392 phosphorylation of p53 as nutlin-3 treatment did (Fig. S3*G*).

On the other hand, overexpression of STING suppressed the Ser392 phosphorylation of p53 induced by nutlin-3 or CDDP treatment in the U2OS cells (Fig. 4*G* and Fig. S3*H*). Similarly, overexpression of STING also suppressed Ser392 phosphorylation of p53 induced by nutlin-3 in A549 cells or by IFN-γ in HaCaT cells (Fig. 4*H* and Fig. S3*I*). In addition, we observed that IFI16 and Ser392-phosphorylated p53 colocalized in the nucleus, and more depolarized mitochondria were detected in the nutlin-3–treated and IFI16-overexpressed cells (Fig. S4*A*), which was consistent with more apoptosis and more loss of $\Delta\Psi_m$ in these cells. When IFI16 was deleted or STING was stably overexpressed, nutlin-3–induced Ser392 phosphorylation of p53 was restrained, and mitochondria damage was reduced (Fig. S4, *B* and *C*).

Together, IFI16 facilitates and STING suppresses Ser392 phosphorylation of p53 in U2OS and A549 cells, which suggests that Ser392-phosphorylated p53 potentially mediates the effect of IFI16 on the regulation of apoptosis, the loss of $\Delta\Psi_m$, and p53 transcriptional activity.

Ser392 phosphorylation of p53 is required for the IFI16-p53–dependent apoptosis

To confirm the function of Ser392 phosphorylation of p53 in apoptosis, we compared the WT p53 and p53(S392A), with a mutation at serine 392 to alanine. Nutlin-3 and IFN-γ cotreatment or CDDP single treatment dramatically induced apoptosis in U2OS cells (Fig. 5, *A* and *B*). WT p53 expression further facilitated apoptosis levels, whereas the p53(S392A) induced apoptosis in these cells to a lesser extent (Fig. 5, *A* and *B*). Gradual elevation of Ser392-phosphorylated p53 was detected in the WT p53 expressed cells rather than in the p53(S392A) expressed cells, along with increased levels of WT or mutated p53 (Fig. 5*C*). Consistently, less apoptosis induction was observed in the p53(S392A)-rescued than that in WT p53-rescued NCI-H1299 cells (Fig. 5*D*). WT p53 rescued in NCI-H1299 cells facilitated nutlin-3–induced IFI16 and cleaved caspase 3 expression (Fig. 5*E*), whereas much less cleaved caspase 3 was detected in the p53(S392A) transfected NCI-H1299 cells as a result of a defect in Ser392 phosphorylation (Fig. 5*E*). Consistent with the apoptosis results, less $\Delta\Psi_m$ loss and lower p53 transcriptional activity were observed in the p53(S392A)-transfected cells than that in the WT p53-transfected cells (Fig. 5, *F* and *G*).

By reconstruction of the functional p53 signaling pathway in U2OS and NCI-H1299 cells, our results suggest that the Ser392 phosphorylation of p53 induced by IFI16 is critical for the regulation of apoptosis, the loss of $\Delta\Psi_m$, and p53 transcriptional activity.

STING-mediated IFI16 degradation suppresses p53-dependent apoptosis

Our previous study has proved that STING facilitates IFI16 degradation *via* the ubiquitin–proteasome system (7). In U2OS cells, we also observed that stably expressed STING suppressed the induction of apoptosis in the *WT* cells rather than in the *IFI16*$^{-/-}$ cells (Fig. 6*A*). STING dramatically suppressed the inducible IFI16 protein levels and also suppressed IFI16-p53–dependent apoptosis in the nutlin-3–treated cells (Fig. S3*C* and Fig. 6, *B* and *C*). Similarly, overexpression of STING suppressed the loss of $\Delta\Psi_m$ in the *WT* cells but not in the *IFI16*$^{-/-}$ cells (Fig. 6*D*). STING stable expression and knockout of IFI16 also suppressed the level of basal and inducible p53 target genes *PUMA* and *BAX* expression, indicating their roles in regulating mitochondrial pathway–associated apoptosis (Fig. 6, *E* and *F*).

IFI16-K3/4/6R, an IFI16 mutant that is resistant to STING-mediated degradation (7), more effectively facilitated the Ser392 phosphorylation of p53, the induction of p53 target genes such as *PUMA* and *BAX*, and p53-dependent apoptosis in A549 cells (Fig. 6, *G–I*). In addition, more *PUMA* mRNA was induced in the *IFI16*$^{-/-}$ HaCaT cells rescued by IFI16-K3/4/6R than WT IFI16 (Fig. S5). As a result, IFI16-K3/4/6R
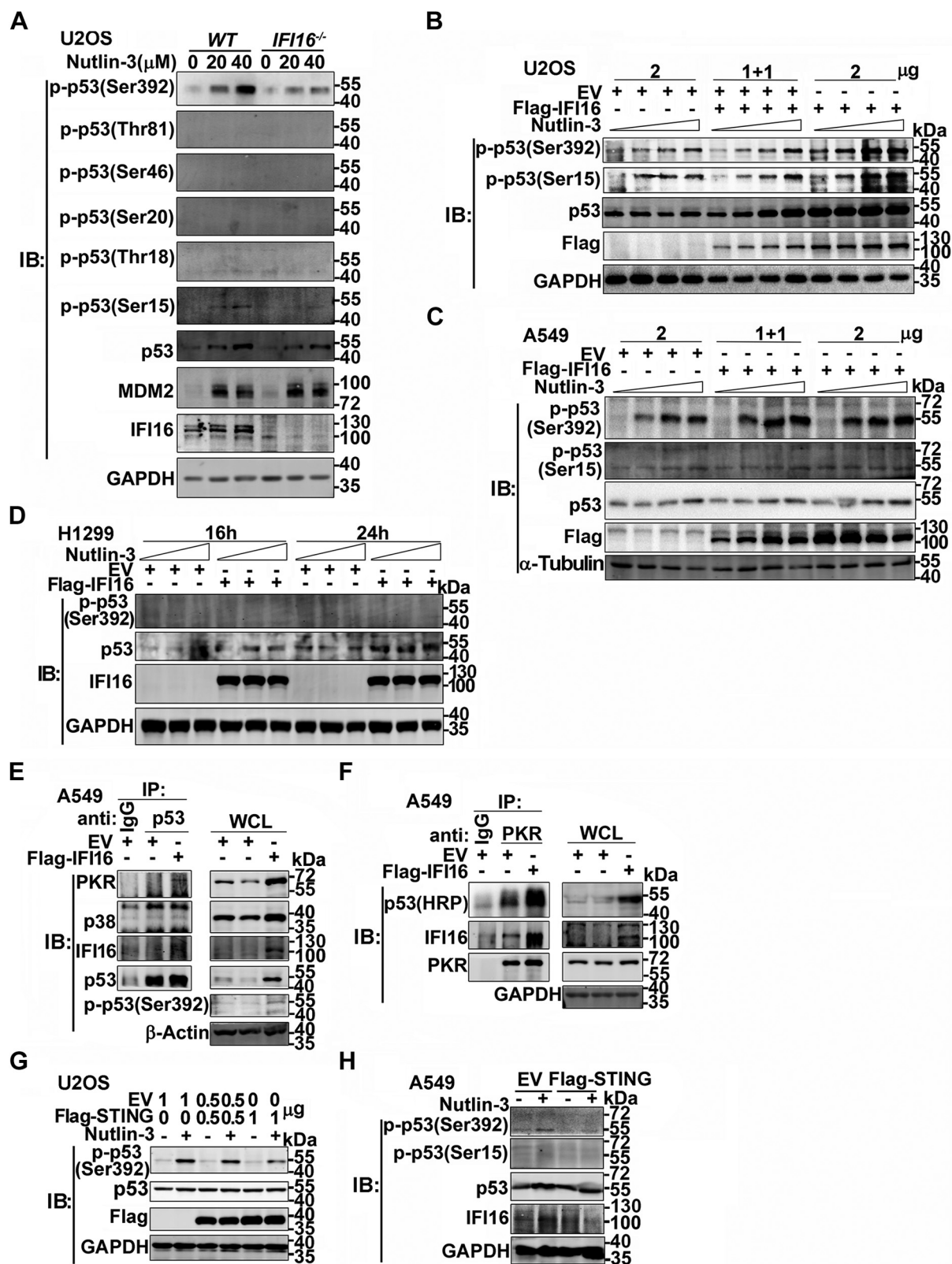
Figure 4. IFI16 and STING perform opposite effects in the regulation of PKR-mediated Ser392 phosphorylation of p53. *A*, *WT* and *IFI16−/−* U2OS cells plating in 6-well plates were treated with nutlin-3 for 24 h. The whole cell lysates (WCLs) were subjected to IB analysis with indicated antibodies. *B–D*, EV (2 μg) or Flag-IFI16 (2 μg) vector-transfected U2OS (*B*), A549 (*C*), or NCI-H1299 (*D*) cells (6-well plate) were treated with nutlin-3 (0–20 μM) for 24 h. The WCLs were subjected to IB analysis with indicated antibodies. *E* and *F*, A549 cells in 100-mm dishes were transfected with EV or Flag-IFI16 vectors (10 μg) for 32 h. Total cell lysates were immunoprecipitated (IP) with mouse anti-p53 antibody and total mouse IgG antibody as control (*E*) or rabbit anti-PKR antibody and total rabbit IgG antibody as control (*F*). The immunoprecipitates or WCL were subjected to IB analysis with indicated antibodies. *G* and *H*, EV (1 μg) or Flag-STING (1 μg) vector-transfected U2OS (*G*) or A549 (*H*) cells (6-well plates) were treated with nutlin-3 (30 μM) for 18 h. The WCL was subjected to IB analysis with indicated antibodies. EV, empty vector; IB, immunoblot; IFI16, interferon-γ–inducible factor 16; PKR, protein kinase R; Ser392, serine 392; STING, stimulator of interferon genes.
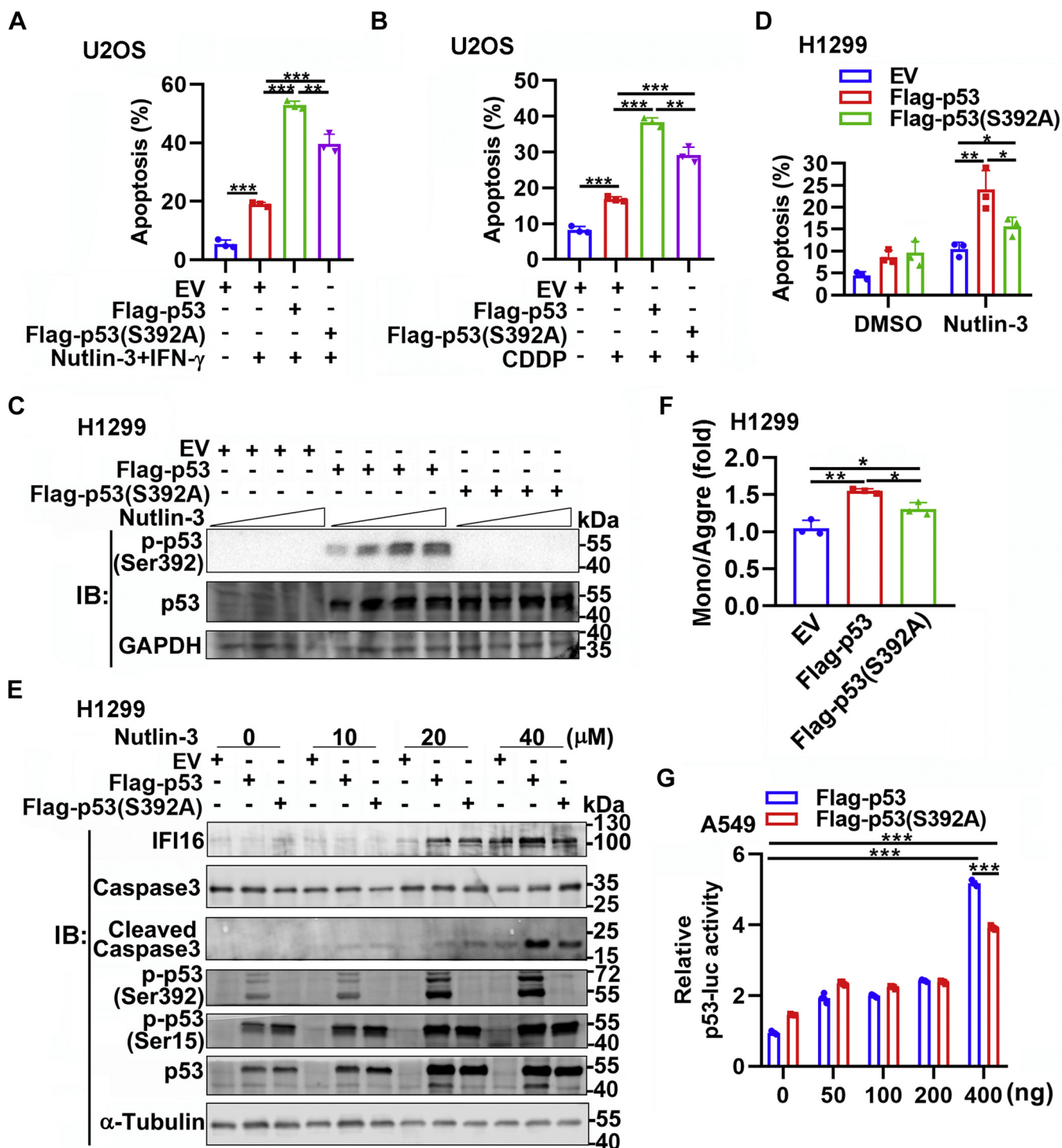
Figure 5. Ser392 phosphorylation is critical for p53-dependent apoptosis in tumor cells. *A* and *B*, EV (1 μg), Flag-p53 (1 μg), or Flag-p53(S392A) (1 μg) vector-transfected U2OS cells (12-well plates) were treated with nutlin-3 (*A*, 30 μM) and IFN-γ (*A*, 20 ng/ml) or CDDP (*B*, 50 μM) for 24 h, and the cells were harvested by trypsin digestion and stained with annexin V/PI for apoptosis analysis by flow cytometry. *C–E*, EV (1 μg), Flag-p53 (1 μg), or Flag-p53(S392A) (1 μg) vector-transfected NCI-H1299 cells (12-well plates) were treated with nutlin-3 (*C*, 0–20 μM; *D*, 40 μM; *E*, indicated concentration) for 24 h. The whole cell lysates from (*C* and *E*) were subjected to IB analysis with indicated antibodies, and the cells from (*D*) were harvested by trypsin digestion and stained by annexin V/PI for apoptosis analysis. *F*, EV (1 μg), Flag-p53 (1 μg), or Flag-p53(S392A) (1 μg) vector-transfected NCI-H1299 cells (12-well plate) were harvested by trypsin digestion and stained with JC-1 dye for ΔΨ$_m$ analysis by flow cytometry. *G*, A549 cells in 24-well plates were cotransfected with p53-luc (150 ng) and the indicated dose of Flag-p53/Flag-p53(S392A)–expressing plasmids, relative firefly luciferase activity was quantified 24 h after transfection. The experiment was repeated three times, and the data in (*A*, *B*, *D*, *F*, and *G*) are expressed as mean ± SD (*$p < 0.05$, **$p < 0.01$, ***$p < 0.001$; unpaired Student's *t* test). EV, empty vector; IB, immunoblot; IFN-γ, interferon gamma; p53-luc, a p53 luciferase reporter; PI, propidium iodide; Ser392, serine 392.
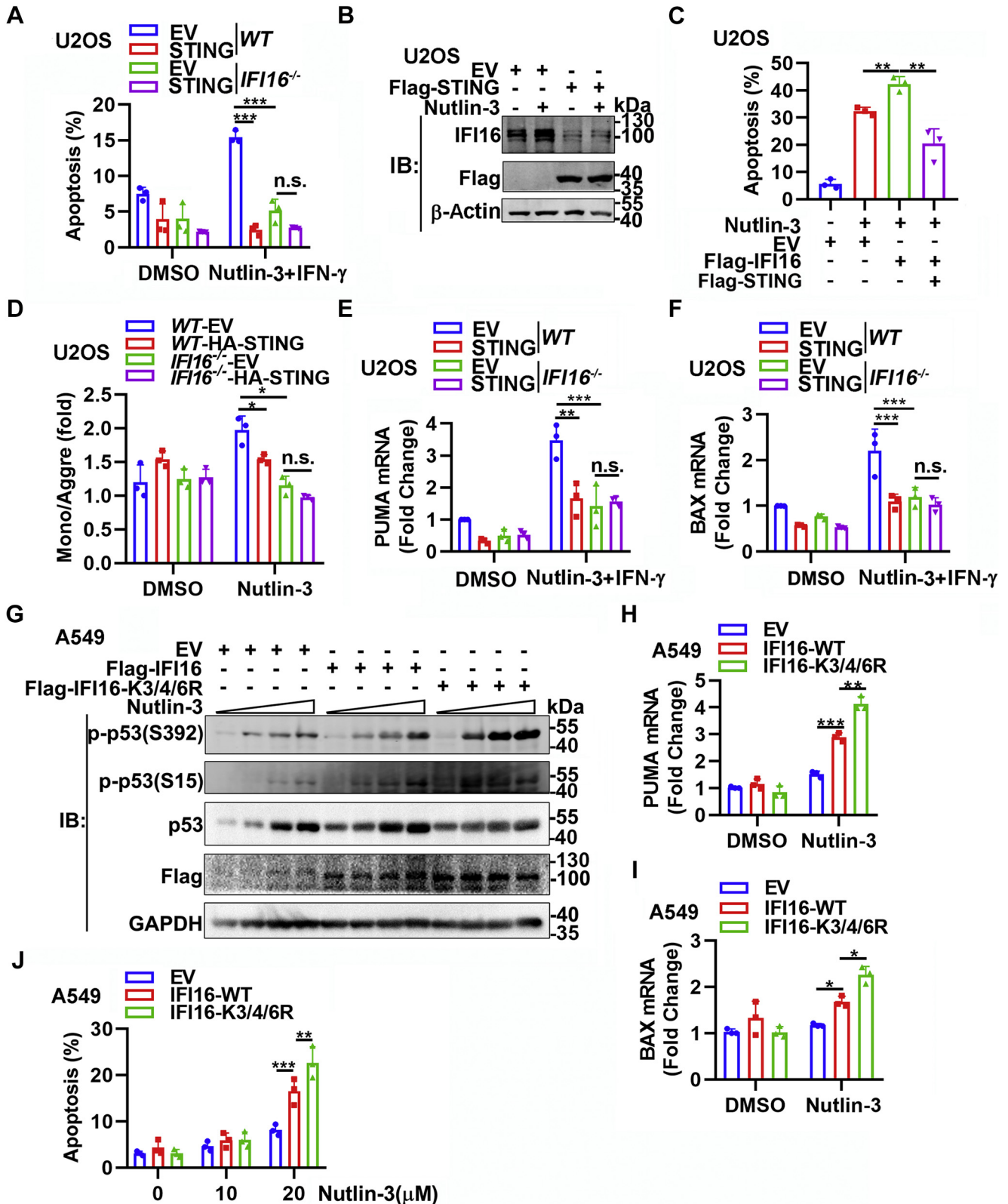
Figure 6. STING-mediated IFI16 degradation suppresses IFI16-p53–dependent apoptosis. *A*, WT, WT-STING, IFI16^{−/−}, and IFI16^{−/−}-STING monoclonal cell lines were treated with DMSO or nutlin-3 (30 μM) and IFN-γ (20 ng/ml) for 18 h. Apoptotic cells were analyzed by flow cytometry. *B* and *C*, U2OS cells in 6-well plates were transfected with EV (0.5 μg in *B*, 2 μg in *C*), Flag-STING (0.5 μg), or Flag-IFI16 (2 μg) vectors as indicated for 8 h and then treated with nutlin-3 (40 μM) for 24 h. The whole cell lysates from (*B*) were subjected to IB analysis with indicated antibodies, and the cells from (*C*) were harvested by trypsin digestion and stained with annexin V/PI for apoptosis analysis by flow cytometry. *D*, WT or IFI16^{−/−} U2OS cells were transfected with EV (0.5 μg), or Flag-STING (0.5 μg) vectors and treated with nutlin-3 (40 μM). About 20 h after transfection, the cells were harvested by trypsin digestion and stained with JC-1 dye for ΔΨ$_m$ analysis by flow cytometry. *E* and *F*, WT, WT-STING, IFI16^{−/−}, and IFI16^{−/−}-STING monoclonal cell lines were treated with nutlin-3 (40 μM) and IFN-γ (20 ng/ml) treatment for 16 h. The mRNA expression level of *PUMA* and *BAX* were measured by RT-quantitative PCR. *G–J*, EV (1 μg), Flag-IFI16

overexpression leads to more apoptosis than WT IFI16 in A549 cells (Fig. 6*J*).

In summary, our results have indicated that IFI16 promotes p53-dependent apoptosis, the loss of $\Delta\Psi_m$, Ser392 phosphorylation of p53, p53 transcriptional activity, and expression of p53 target genes in U2OS and A549 cells. However, STING inhibits these IFI16-mediated effects by promoting the degradation of the upstream IFI16 (Fig. 7).

Discussion

IFI16 is an important regulator in both antiviral immunity and tumorigenesis. Alternation of IFI16 expression level is associated with multiple diseases including autoimmune diseases and cancers. Comparing with healthy people, significantly higher level of IFI16 mRNA in peripheral blood mononuclear cells and much more cases with autoantibodies against IFI16 in serum are detected in the patients with systemic lupus erythematosus (33). In addition, high levels of circulating IFI16 and anti-IFI16 antibodies are prevalent in the sera of patients with Sjögren's syndrome (34). In contrast to the increased level of IFI16 in autoimmune diseases, loss or reduced expression of IFI16 is often correlated with various forms of human cancers, including those of osteo-sarcoma, prostate cancer, breast cancer, and melanoma (10, 35–37). Increased expression of IFI204, the murine homolog of human IFI16, is associated with decreased melanoma growth in murine models, and higher expression of IFI16 is correlated with prolonged survival of patients with melanoma (36). IFI16 expression is tightly controlled to maintain homeostasis during antiviral immunity. High level of IFI16 triggers strong IFN-I–dependent antiviral immunity, following by the overactivation of host innate immunity, which leads to autoimmunity. Negative feedback degradation of IFI16 mediated by STING–tripartite motif–containing protein 21 complex attenuates antiviral immunity and protects cells from self-injury (7). However, the down-regulation of IFI16 suppresses p53-dependent apoptosis, which may potentially lead to tumorigenesis. Our current study has suggested a detrimental role of STING-mediated degradation of IFI16 in tumorigenesis, although it is bene-ficial for the host to avoid autoimmunity during antiviral immunity.

The p53 tumor suppressor protein plays a major role in cellular response to DNA damage and other genomic aberra-tions. Activation of p53 by phosphorylation at multiple sites triggers apoptosis pathway and inhibits tumorigenesis (38). The C-terminal phosphorylation of p53 is less studied than those of its N-terminal region. At least four sites (Ser315, Ser366, Ser378, and Ser392) constitute the C-terminal phos-phorylation region (39, 40). Among these, Ser392 is highly conserved in vertebrates. Phosphorylation of p53 at Ser392 is required for the growth suppressor function, DNA binding, and transcriptional activity of p53 (11, 12, 41). In addition, Ser392 phosphorylation drives p53 mitochondrial trans-location and transcription-independent apoptosis in lung cancers (42). Low-dose nutlin-3a combined with actinomycin D synergistically activates p53 but cannot induce apoptosis (43). In our study, we have found that high-dose nutlin-3 is able to trigger p53-dependent apoptosis and to induce IFI16 expression. IFI16 recruits PKR to p53, which induces Ser392 phosphorylation of p53, even in the absence of nutlin-3. Knockout of IFI16 downregulates the transcriptional activity of p53 and the induction of p53 target genes, such as *PUMA* and *BAX*, which are responsible for mitochondria-dependent apoptosis. Meanwhile, less loss of $\Delta\Psi_m$ is detected in the nutlin-3–treated *IFI16*$^{-/-}$ cells. Besides the function of Ser392 phosphorylation in inducing transcription-independent apoptosis, our results suggest that IFI16 promotes PKR-mediated Ser392 phosphorylation of p53 and p53-dependent apoptosis *via* the transcription-dependent pathway, which induces p53 target genes and leads to increased mitochondrial permeability. However, the maximal activation of p53 was synergistically controlled by various phosphorylation sites as the mutation at Ser392 only partially restrains p53-dependent function.

Although STING agonists have been extensively used in cancer therapy studies and clinical trials (18, 19, 44), there are some findings showing different functions of STING signaling in tumorigenesis. Several studies have described the protumor role of STING by activating its downstream IFN-I or NF-κB signaling (21, 22). Cyclic GMP–AMP synthase, the upstream DNA sensor of STING, could translocate into the nucleus, suppress homologous recombination–mediated repair, and promote tumor growth (45). IFI16 cooperates with cyclic GMP–AMP synthase to activate STING during DNA sensing in human keratinocytes (46). Our results have indicated that STING-mediated IFI16 degradation suppresses Ser392-phosphorylated p53 and p53-dependent apoptosis in *WT* U2OS cells rather than in *IFI16*$^{-/-}$ cells, suggesting that STING also may promote tumorigenesis by negatively regu-lating the upstream IFI16-p53 apoptosis signaling. The phys-iological functions of STING-mediated IFI16 degradation in tumorigenesis will be further investigated by using the IFI16-K3/4/6R rescued tumor cells and related xenografted tumor mouse models.

Considering that DNA from the genome of tumorigenic viruses such as Epstein–Barr virus, human papillomavirus, and Kaposi sarcoma–associated herpesvirus is recognized by IFI16 (5, 47, 48), downregulation of IFI16 by viral proteins or host intrinsic regulators such as STING potentially inhibit IFI16-p53–dependent apoptosis, which may eventually lead to
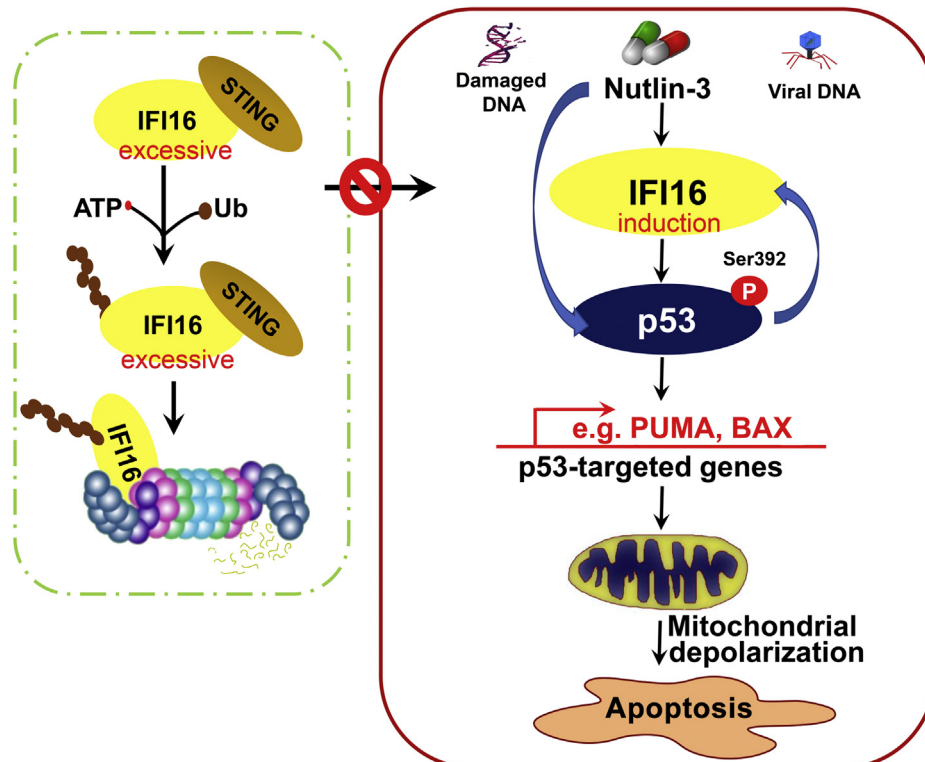
Figure 7. Working model. The IFI16-p53 positive feedback regulation promotes Ser392 phosphorylation of p53, p53 transcriptional activity, p53 target gene expression, the loss of $\Delta\Psi_m$, and the p53-dependent apoptosis in tumor cells. However, STING-mediated degradation of the accumulated IFI16 restrains these IFI16-p53–dependent effects. IFI16, interferon-γ–inducible factor 16; Ser392, serine 392; STING, stimulator of interferon genes.

tumorigenesis. STING-mediated degradation of IFI16 benefits the host cells to avoid excessive IFN-I production and autoimmunity during antiviral immunity against these tumorigenic viruses. However, this negative regulation also blocks p53-dependent apoptosis, which may account for the tumorigenic activity of some DNA viruses. Several nutlin family antagonists blocking p53–MDM2 binding including RG7112 and RG7388 have been undergoing clinical investigation (49–51). IFI16 can be induced by damaged DNA or transcriptional activation. Our current findings imply that the traditional chemotherapy, radiotherapy, or p53–MDM2 target antagonist therapies may suffer a restraining in some tumors like osteosarcoma or NSCLC with high STING expression levels, which counteract p53-dependent tumor cell apoptosis. This study also provided an alternative strategy to avoid tumorigenesis during tumor viral infection, that is, ensuring enough IFI16 stabilization or Ser392-phosphorylated p53, *via* the inhibitors to avoid IFI16 degradation combined with nutlin family antagonist treatment.

Experimental procedures

Cell lines and reagents

Human NSCLC A549 cells and human embryonic kidney 293T (HEK293T) cells were purchased from American Type Culture Collection. Human osteosarcoma U2OS cells, human NSCLC cells NCI-H1299, and human large cell lung cancer cell line NCI-H460 were purchased from the Cell Bank of Chinese Academy of Sciences. *WT* and *IFI16*$^{-/-}$ keratinocyte

HaCaT cells were generously provided by Professor Leonie Unterholzner (University of Edinburgh). A549 and HaCaT cells were cultured in Dulbecco's modified Eagle's medium, and the resting cell lines were cultured in RPMI1640, supplemented with 10% heat-inactivated fetal bovine serum, 100 units/ml penicillin, and 100 μg/ml streptomycin, at 37 °C and 10% CO_2. For apoptosis assay and mitochondrial membrane potential assay, A549 and NCI-H1299 cells were cultured with 5% fetal bovine serum when nutlin-3 was added into the medium. Primary anti-IFI16 antibody (#sc-8023) and mouse anti-p-p53 (Ser392) antibody (#sc-51690) were purchased from Santa Cruz Biotechnology. Mouse anti-STING antibody (MABF270) was purchased from Millipore. Rabbit anti-STING antibody (#13647), rabbit anti-p-p53 (Ser392) antibody (#9281), anti-p53 (Thr81) antibody (#2676T), anti-p-p53 (Ser46) antibody (#2521T), anti-p-p53 (Ser20) antibody (#9287T), anti-p-p53 (Thr18) antibody (#2529T), anti-p-p53 (Ser15) antibody (#9284), anti-p53 antibody (#2524), anti-MDM2 antibody (#86934), anti-caspase 3 antibody (#9662), anti-cleaved caspase 3 antibody (#4199), anti-p38 antibody (#8690), anti-hemagglutinin horse radish peroxidase (HRP)–conjugated antibody (#2999), and anti-GAPDH antibody (#5174) were purchased from Cell Signaling Technology. Anti-p53 (HRP) antibody (#ab204452) and anti-PKR antibody (#ab32052) were purchased from Abcam. Anti-α-Tubulin antibody (#5168), anti-Flag antibody (#F1804), and HRP-conjugated anti-Flag antibody (#A8592) were purchased from Sigma–Aldrich. Anti-mouse IRDye800CW

secondary antibody (#926-32212), anti-rabbit IRDye800CW secondary antibody (#926-32213), anti-mouse IRDye680RD secondary antibody (#926-68072), and anti-rabbit IRDye680RD secondary antibody (#926-68073) were purchased from LI-COR. Recombinant human IFN-γ was purchased from InvivoGen, CDDP was obtained from Beyotime Biotechnology, and nutlin-3 was purchased from Selleck.

Generation of IFI16$^{−/−}$ U2OS cells and STING stably expressing cell lines

U2OS single clonal cells lacking *IFI16* were generated using CRISPR/Cas9 technology (52, 53). Two separate single guide RNAs targeting *IFI16* were inserted into the lentiCRISPR v2 vectors expressing a Cas9 gene (Addgene; #52961). The following were the two single guide RNA targeting sequences: #1, 5′-TATACCAACGCTTGAAGACC-3′; #2, 5′-CCACA AGCAGCACTGTCAAA-3′. Lenti-CRISPR virions were produced by transfecting HEK293T cells with the following plasmids: CRISPR/Cas9 vector, pMD.2G, pRSV-REV, and pMDlg/p-RRE. Viral supernatants were harvested after 72 h and used to infect U2OS cells in the presence of 6 μg/ml polybrene (EMD Millipore). Transduced cells were selected with 4 μg/ml puromycin (InvivoGen) at 48 h after transduction. After 4 weeks of selection, single cell clones were established and subjected to genotyping and immunoblotting to confirm the deletion of IFI16 expression and the homogeneity of each cell clone. The STING stably expressing cells were generated based on the *WT* and *IFI16$^{−/−}$* U2OS cell lines. In brief, the hemagglutinin-STING–expressing plasmid with a pcDNA3.1 backbone was transfected into U2OS cells. Transfected cells were selected with 800 μg/ml G418 (Thermo Fisher Scientific) at 48 h after transfection. After 4 weeks of selection, single-cell clones were established and subjected to Western blotting to confirm the expression of STING of each clone.

Construction and mutation of vectors

All the WT IFI16, STING, and p53 plasmids were gifts from Professor Genhong Cheng (University of California). The Flag-p53(S392A) vectors were generated by PCR amplification using a pair of oligonucleotide primers (forward: 5′-CCG CTCGAGCGATGGACTACAAGGACGACGATGACAAG-3′, reverse: 5′- GCGGGATCCTCAGTCTGCGTCAGGCCCTTC TGTCTTG-3′) and WT p53 plasmid as templates by subcloning. The Flag-IFI16-K3/4/6R mutants were generated in the previous study (7). The sequence of all constructs was verified by Sanger DNA sequencing and immunoblotting.

Cell transfection and stimulation

Transient transfection of plasmids was performed with polyethylenimine (Polysciences) into different cell lines according to the manufacturer's instructions. Plasmids were transfected into A549, NCI-H1299, and NCI-H460 cells at the ratio of 3 μl:1 μg (reagents/DNA), into U2OS cells at the ratio of 2 μl:1 μg (reagents/DNA), into HEK293T cells at the ratio of

1 μl:1 μg (reagents/DNA). Cells were treated with nutlin-3, CDDP, or IFN-γ as indicated in the figure legends.

Mitochondrial membrane potential (ΔΨ$_m$) analysis by JC-1 staining

For monitoring the loss of ΔΨ$_m$ in early apoptotic cells, A549/U2OS cell lines pretreated as indicated in the figure legends were harvested by trypsin and stained by JC-1 dye according to the manufacturer's instruction (Meilunbio). JC-1 is predominantly aggregated with a red to orange fluorescence in cells with high ΔΨ$_m$ (Fig. 2A, *green spots*). When cells become apoptosis caused by mitochondrial depolarization or ΔΨ$_m$ loss, the dye yields monomers with green fluorescence (Fig. 2A, *red spots*). The percentage of green/red fluorescence-positive cells was analyzed on an Attune NxT Acoustic Focusing Cytometer (ThermoFisher Scientific). The loss of cellular ΔΨ$_m$ was indicated by an increase in the green/red fluorescence–positive (monomers/aggregates) cell ratio.

Apoptosis analysis by FITC–annexin V and propidium iodide staining

For monitoring IFI16-p53 signaling–associated cell apoptosis, U2OS cells, A549 cells, or NCI-H1299 cells pretreated as indicated in the figure legends were harvested by trypsin and analyzed by flow cytometry using FITC–annexin V and propidium iodide staining kit according to the manufacturer's instruction (BD Pharmingen). Apoptotic cells were identified as annexin V$^+$ on an Attune NxT Acoustic Focusing Cytometer.

Cell viability analysis by Cell Counting Kit-8

Seed cells in 96-well plates and transfect the cells with empty vector, Flag-IFI16, or Flag-STING vectors. About 8 h post transfection, nutlin-3 was added into the medium for 24 h. Discard the old medium and add Cell Counting Kit-8 (Dojindo) solution containing medium to each well of the plates. Incubate the plate for 2 h and measure the absorbance at 450 nm using a microplate reader.

Quantitative real-time PCR

Total RNA was extracted using the RNeasy Mini Kit from QIAGEN (Hilden), and complementary DNA was synthesized using the PrimeScript RT Master Mix (Takara). Quantitative real-time PCR amplification was performed using TB Green Premix Ex Taq (Tli RNaseH Plus; Takara) on a Roche Light-Cycler 480 II system. The relative mRNA expression level of genes was normalized to the internal control ribosomal protein *RPL32* gene by using $2^{−ΔΔCt}$ cycle threshold method (54). The primer sequences for quantitative PCR were from primer bank (55), and they are available upon request.

Immunoblotting

Whole cell lysates were prepared in lysis buffer (50 mM Tris–HCl, pH 7.5, 150 mM NaCl, 1% [v/v] Nonidet P-40, and 0.5 mM EDTA) supplemented with cOmplete Protease

Inhibitor Cocktail (Roche). For phosphorylation detection, the lysis buffer was supplemented with Roche PhosSTOP (Roche). The total cell lysate was subjected to SDS-PAGE, and immunoblot analysis was performed with indicated primary antibodies and the LI-COR IRDye secondary antibodies. The antigen–antibody complexes were visualized by chemiluminescence (ECL, Millipore) on Bio-Rad ChemiDoc XRS+ system or directly by Odyssey CLx Imaging System (LI-COR).

Mitochondrial staining

To test whether nutlin-3 and IFI16 lead to mitochondrial depolarization, Mito-Tracker Red CMXRos (Beyotime Biotechnology) was used for mitochondrial staining according to the manufacturer's instruction. Briefly, discard the culture medium and wash cells two times with nonserum culture medium. The 37 °C preheated Mito-Tracker Red CMXRos working solution was directly added into living cells seeded on glass coverslips, 37 °C, and 20 min. After staining, the cells were washed with PBS three times and then stained by 4′,6-diamidino-2-phenylindole (DAPI) or antibodies for immunofluorescence detection.

Immunofluorescence

Pretreated A549 or U2OS cells plated on glass coverslips were fixed using 4% formaldehyde for 20 min and permeabilized with 0.2% Triton-X100 for 10 min. Next, the cells were blocked and incubated with rabbit anti-p-p53 (Ser392), mouse anti-Flag, mouse anti-IFI16, or mouse anti-STING primary antibodies overnight. After washing three times with PBS, cells were incubated with secondary antibodies to each of the primary antibodies for 1 h, and the cells were washed with PBS three times and then stained by DAPI. Slides were evaluated using a LEICA TCA SP8 confocal microscope (Leica Microsystems). Cell images obtained were exported using the LCS software package into tag image file format for further analysis.

In situ *proximity ligation assay*

Duolink *In Situ* Proximity Ligation Assay Detection Kit (Sigma–Aldrich) was used to identify endogenous p38 or PKR-mediated Ser392 phosphorylation on p53. Pretreated A549 cells plated on glass coverslips were fixed using 4% formaldehyde for 20 min and permeabilized with 0.2% Triton-X100 for 10 min. The fixed cells were blocked and incubated with mouse anti-p-p53 (Ser392) and rabbit anti-PKR primary antibodies overnight. In the next steps, incubation of secondary antibodies, ligation, and signal amplification were finished according to the manufacturer's instructions. When the two primary antibodies are in close enough proximity, the amplification will generate a signal (red spot). After DAPI staining, cells were detected on a LEICA TCA SP8 confocal microscope. Images were exported using the LCS software package into tag image file format. Cellular interaction signals were determined by ImageJ software (Laboratory for Optical and Computational Instrumentation) for statistical analysis.

Firefly luciferase reporter assay

A549 or U2OS cell lines were seeded in 24-well plates at a density of 1.0×10^5 cells per well and cultured for 24 h. The cells were transfected with a mixture of p53 firefly luciferase reporter plasmid (p53-luc) and other indicated plasmids using polyethylenimine transfection reagents. After 8 h, the transfection medium was replaced with fresh medium with or without nutlin-3. About 24 h or 32 h (indicated in the figure legends) after transfection, cells were lysed and luciferase activity was measured using the Luciferase Reporter Assay System (Promega) according to the manufacturer's instruction.

Statistics

The number of experimental repeats are shown in figure legends. All bar graphs are shown as means with SD. Statistical analysis was performed with Student's t test in GraphPad Prism 8 software (GraphPad Software, Inc). p Value less than 0.05 was considered significant. $*p < 0.05$, $**p < 0.01$, and $***p < 0.001$.

Data availability

All the data are contained in the article and supporting information.

Author contributions—F. M. conceptualization; D. L. and L. X. data curation; D. L. and S. M. formal analysis; D. L. and F. M. funding acquisition; D. L., L. X., Z. Q., J. Z., F. Z., S. C., L. L., and H. Y. investigation; D. L. writing–original draft; D. L. and F. M. writing–review and editing; L. X. and Z. Q. methodology; F. S., Y. Q., S. H., and F. M. resources.

Abbreviations—The abbreviations used are: BAX, Bcl-2–associated X protein; CDDP, cisplatin; DAPI, 4′,6-diamidino-2-phenylindole; HEK293T, human embryonic kidney 293T; HIN, hematopoietic expression, IFN-inducible, and nuclear location; HRP, horse radish peroxidase; IFN, interferon; IFN-I, type I IFN; IFI16, interferon-γ–inducible factor 16; MDM2, murine double minute 2; NSCLC, non–small cell lung cancer; p53-luc, a p53 luciferase reporter; PKR, protein kinase R; PUMA, p53 upregulated modulator of apoptosis;

STING negatively regulates IFI16-p53–dependent apoptosis

PYD, PYRIN domain; Ser15, serine 15; Ser392, serine 392; STING, stimulator of interferon genes.

References

1. Unterholzner, L., Keating, S. E., Baran, M., Horan, K. A., Jensen, S. B., Sharma, S., Sirois, C. M., Jin, T., Latz, E., Xiao, T. S., Fitzgerald, K. A., Paludan, S. R., and Bowie, A. G. (2010) IFI16 is an innate immune sensor for intracellular DNA. *Nat. Immunol.* **11**, 997–1004
2. Choubey, D., Duan, X., Dickerson, E., Ponomareva, L., Panchanathan, R., Shen, H., and Srivastava, R. (2010) Interferon-inducible p200-family proteins as novel sensors of cytoplasmic DNA: Role in inflammation and autoimmunity. *J. Interferon Cytokine Res.* **30**, 371–380
3. Dawson, M. J., and Trapani, J. A. (1996) HIN-200: A novel family of IFN-inducible nuclear proteins expressed in leukocytes. *J. Leukoc. Biol.* **60**, 310–316
4. Stehlik, C. (2007) The PYRIN domain in signal transduction. *Curr. Protein Pept. Sci.* **8**, 293–310
5. Kerur, N., Veettil, M. V., Sharma-Walia, N., Bottero, V., Sadagopan, S., Otageri, P., and Chandran, B. (2011) IFI16 acts as a nuclear pathogen sensor to induce the inflammasome in response to Kaposi Sarcoma-associated herpesvirus infection. *Cell Host Microbe* **9**, 363–375
6. Dowling, J. K., and O'Neill, L. A. (2012) Biochemical regulation of the inflammasome. *Crit. Rev. Biochem. Mol. Biol.* **47**, 424–443
7. Li, D., Wu, R., Guo, W., Xie, L., Qiao, Z., Chen, S., Zhu, J., Huang, C., Huang, J., Chen, B., Qin, Y., Xu, F., and Ma, F. (2019) STING-mediated IFI16 degradation negatively controls type I interferon production. *Cell Rep.* **29**, 1249–1260.e1244
8. Choubey, D., and Panchanathan, R. (2016) IFI16, an amplifier of DNA-damage response: Role in cellular senescence and aging-associated inflammatory diseases. *Ageing Res. Rev.* **28**, 27–36
9. Liao, J. C., Lam, R., Brazda, V., Duan, S., Ravichandran, M., Ma, J., Xiao, T., Tempel, W., Zuo, S., Wang, Y. X., Chirgadze, N. Y., and Arrowsmith, C. H. (2011) Interferon-inducible protein 16: Insight into the interaction with tumor suppressor p53. *Structure* **19**, 418–429
10. Fujiuchi, N., Aglipay, J. A., Ohtsuka, T., Maehara, N., Sahin, F., Su, G. H., Lee, S. W., and Ouchi, T. (2004) Requirement of IFI16 for the maximal activation of p53 induced by ionizing radiation. *J. Biol. Chem.* **279**, 20339–20344
11. Bruins, W., Bruning, O., Jonker, M. J., Zwart, E., van der Hoeven, T. V., Pennings, J. L., Rauwerda, H., de Vries, A., and Breit, T. M. (2008) The absence of Ser389 phosphorylation in p53 affects the basal gene expression level of many p53-dependent genes and alters the biphasic response to UV exposure in mouse embryonic fibroblasts. *Mol. Cell. Biol.* **28**, 1974–1987
12. Cox, M. L., and Meek, D. W. (2010) Phosphorylation of serine 392 in p53 is a common and integral event during p53 induction by diverse stimuli. *Cell Signal.* **22**, 564–571
13. Shangary, S., and Wang, S. (2009) Small-molecule inhibitors of the MDM2-p53 protein-protein interaction to reactivate p53 function: A novel approach for cancer therapy. *Annu. Rev. Pharmacol. Toxicol.* **49**, 223–241
14. Herrmann, C. P., Kraiss, S., and Montenarh, M. (1991) Association of casein kinase II with immunopurified p53. *Oncogene* **6**, 877–884
15. Cuddihy, A. R., Wong, A. H., Tam, N. W., Li, S., and Koromilas, A. E. (1999) The double-stranded RNA activated protein kinase PKR physically associates with the tumor suppressor p53 protein and phosphorylates human p53 on serine 392 *in vitro*. *Oncogene* **18**, 2690–2702
16. Huang, C., Ma, W. Y., Maxiner, A., Sun, Y., and Dong, Z. (1999) p38 kinase mediates UV-induced phosphorylation of p53 protein at serine 389. *J. Biol. Chem.* **274**, 12229–12235
17. Marcus, A., Mao, A. J., Lensink-Vasan, M., Wang, L., Vance, R. E., and Raulet, D. H. (2018) Tumor-derived cGAMP triggers a STING-mediated interferon response in non-tumor cells to activate the NK cell response. *Immunity* **49**, 754–763.e754
18. Ramanjulu, J. M., Pesiridis, G. S., Yang, J., Concha, N., Singhaus, R., Zhang, S. Y., Tran, J. L., Moore, P., Lehmann, S., Eberl, H. C., Muelbaier, M., Schneck, J. L., Clemens, J., Adam, M., Mehlmann, J., *et al.* (2018) Design of amidobenzimidazole STING receptor agonists with systemic activity. *Nature* **564**, 439–443
19. Corrales, L., Glickman, L. H., McWhirter, S. M., Kanne, D. B., Sivick, K. E., Katibah, G. E., Woo, S. R., Lemmens, E., Banda, T., Leong, J. J., Metchette, K., Dubensky, T. W., Jr., and Gajewski, T. F. (2015) Direct activation of STING in the tumor microenvironment leads to potent and systemic tumor regression and immunity. *Cell Rep.* **11**, 1018–1030
20. Ho, S. S., Zhang, W. Y., Tan, N. Y., Khatoo, M., Suter, M. A., Tripathi, S., Cheung, F. S., Lim, W. K., Tan, P. H., Ngeow, J., and Gasser, S. (2016) The DNA structure-specific endonuclease MUS81 mediates DNA sensor STING-dependent host rejection of prostate cancer cells. *Immunity* **44**, 1177–1189
21. Lemos, H., Mohamed, E., Huang, L., Ou, R., Pacholczyk, G., Arbab, A. S., Munn, D., and Mellor, A. L. (2016) STING promotes the growth of tumors characterized by low antigenicity via IDO activation. *Cancer Res.* **76**, 2076–2081
22. Chen, Q., Boire, A., Jin, X., Valiente, M., Er, E. E., Lopez-Soto, A., Jacob, L., Patwa, R., Shah, H., Xu, K., Cross, J. R., and Massague, J. (2016) Carcinoma-astrocyte gap junctions promote brain metastasis by cGAMP transfer. *Nature* **533**, 493–498
23. Dawson, M. J., and Trapani, J. A. (1995) IFI 16 gene encodes a nuclear protein whose expression is induced by interferons in human myeloid leukaemia cell lines. *J. Cell. Biochem.* **57**, 39–51
24. Radhakrishna Pillai, G., Srivastava, A. S., Hassanein, T. I., Chauhan, D. P., and Carrier, E. (2004) Induction of apoptosis in human lung cancer cells by curcumin. *Cancer Lett.* **208**, 163–170
25. Yang, S. Y., Li, Y., An, G. S., Ni, J. H., Jia, H. T., and Li, S. Y. (2018) DNA damage-response pathway heterogeneity of human lung cancer A549 and H1299 cells determines sensitivity to 8-chloro-adenosine. *Int. J. Mol. Sci.* **19**, 1587
26. Sivandzade, F., Bhalerao, A., and Cucullo, L. (2019) Analysis of the mitochondrial membrane potential using the cationic JC-1 dye as a sensitive fluorescent probe. *Bio Protoc.* **9**, e3128
27. Li, P. F., Dietz, R., and von Harsdorf, R. (1999) p53 regulates mitochondrial membrane potential through reactive oxygen species and induces cytochrome c-independent apoptosis blocked by Bcl-2. *EMBO J.* **18**, 6027–6036
28. Paek, A. L., Liu, J. C., Loewer, A., Forrester, W. C., and Lahav, G. (2016) Cell-to-cell variation in p53 dynamics leads to fractional killing. *Cell* **165**, 631–642
29. Fischer, M. (2019) Conservation and divergence of the p53 gene regulatory network between mice and humans. *Oncogene* **38**, 4095–4109
30. Miyashita, T., and Reed, J. C. (1995) Tumor suppressor p53 is a direct transcriptional activator of the human bax gene. *Cell* **80**, 293–299
31. Chipuk, J. E., Bouchier-Hayes, L., Kuwana, T., Newmeyer, D. D., and Green, D. R. (2005) PUMA couples the nuclear and cytoplasmic proapoptotic function of p53. *Science* **309**, 1732–1735
32. Kruse, J. P., and Gu, W. (2009) Modes of p53 regulation. *Cell* **137**, 609–622
33. Kimkong, I., Avihingsanon, Y., and Hirankarn, N. (2009) Expression profile of HIN200 in leukocytes and renal biopsy of SLE patients by real-time RT-PCR. *Lupus* **18**, 1066–1072
34. Baer, A. N., Petri, M., Sohn, J., Rosen, A., and Casciola-Rosen, L. (2016) Association of antibodies to interferon-inducible protein-16 with markers of more severe disease in primary Sjogren's syndrome. *Arthritis Care Res.* **68**, 254–260
35. Xin, H., Curry, J., Johnstone, R. W., Nickoloff, B. J., and Choubey, D. (2003) Role of IFI 16, a member of the interferon-inducible p200-protein family, in prostate epithelial cellular senescence. *Oncogene* **22**, 4831–4840
36. Kim, H., Kim, H., Feng, Y., Li, Y., Tamiya, H., Tocci, S., and Ronai, Z. A. (2020) PRMT5 control of cGAS/STING and NLRC5 pathways defines melanoma response to antitumor immunity. *Sci. Transl. Med.* **12**, eaaz5683
37. Zhang, Y., Howell, R. D., Alfonso, D. T., Yu, J., Kong, L., Wittig, J. C., and Liu, C. J. (2007) IFI16 inhibits tumorigenicity and cell proliferation of bone and cartilage tumor cells. *Front. Biosci.* **12**, 4855–4863

ASBMB

38. Vogelstein, B., Lane, D., and Levine, A. J. (2000) Surfing the p53 network. *Nature* **408**, 307–310

39. Ashcroft, M., Kubbutat, M. H., and Vousden, K. H. (1999) Regulation of p53 function and stability by phosphorylation. *Mol. Cell. Biol.* **19**, 1751–1758

40. Ou, Y. H., Chung, P. H., Sun, T. P., and Shieh, S. Y. (2005) p53 C-terminal phosphorylation by CHK1 and CHK2 participates in the regulation of DNA-damage-induced C-terminal acetylation. *Mol. Biol. Cell* **16**, 1684–1695

41. Lohrum, M., and Scheidtmann, K. H. (1996) Differential effects of phosphorylation of rat p53 on transactivation of promoters derived from different p53 responsive genes. *Oncogene* **13**, 2527–2539

42. Castrogiovanni, C., Waterschoot, B., De Backer, O., and Dumont, P. (2018) Serine 392 phosphorylation modulates p53 mitochondrial translocation and transcription-independent apoptosis. *Cell Death Differ.* **25**, 190–203

43. Krzesniak, M., Zajkowicz, A., Gdowicz-Klosok, A., Glowala-Kosinska, M., Lasut-Szyszka, B., and Rusin, M. (2020) Synergistic activation of p53 by actinomycin D and nutlin-3a is associated with the upregulation of crucial regulators and effectors of innate immunity. *Cell Signal.* **69**, 109552

44. Fu, J., Kanne, D. B., Leong, M., Glickman, L. H., McWhirter, S. M., Lemmens, E., Mechette, K., Leong, J. J., Lauer, P., Liu, W., Sivick, K. E., Zeng, Q., Soares, K. C., Zheng, L., Portnoy, D. A., *et al.* (2015) STING agonist formulated cancer vaccines can cure established tumors resistant to PD-1 blockade. *Sci. Transl. Med.* **7**, 283ra252

45. Liu, H., Zhang, H., Wu, X., Ma, D., Wu, J., Wang, L., Jiang, Y., Fei, Y., Zhu, C., Tan, R., Jungblut, P., Pei, G., Dorhoi, A., Yan, Q., Zhang, F., *et al.* (2018) Nuclear cGAS suppresses DNA repair and promotes tumorigenesis. *Nature* **563**, 131–136

46. Almine, J. F., O'Hare, C. A., Dunphy, G., Haga, I. R., Naik, R. J., Atrih, A., Connolly, D. J., Taylor, J., Kelsall, I. R., Bowie, A. G., Beard, P. M., and Unterholzner, L. (2017) IFI16 and cGAS cooperate in the activation of STING during DNA sensing in human keratinocytes. *Nat. Commun.* **8**, 14392

47. Lo Cigno, I., De Andrea, M., Borgogna, C., Albertini, S., Landini, M. M., Peretti, A., Johnson, K. E., Chandran, B., Landolfo, S., and Gariglio, M. (2015) The nuclear DNA sensor IFI16 acts as a restriction factor for human papillomavirus replication through epigenetic modifications of the viral promoters. *J. Virol.* **89**, 7506–7520

48. Pisano, G., Roy, A., Ahmed Ansari, M., Kumar, B., Chikoti, L., and Chandran, B. (2017) Interferon-gamma-inducible protein 16 (IFI16) is required for the maintenance of Epstein-Barr virus latency. *Virol. J.* **14**, 221

49. Ray-Coquard, I., Blay, J. Y., Italiano, A., Le Cesne, A., Penel, N., Zhi, J., Heil, F., Rueger, R., Graves, B., Ding, M., Geho, D., Middleton, S. A., Vassilev, L. T., Nichols, G. L., and Bui, B. N. (2012) Effect of the MDM2 antagonist RG7112 on the P53 pathway in patients with MDM2-amplified, well-differentiated or dedifferentiated liposarcoma: An exploratory proof-of-mechanism study. *Lancet Oncol.* **13**, 1133–1140

50. Ding, Q., Zhang, Z., Liu, J. J., Jiang, N., Zhang, J., Ross, T. M., Chu, X. J., Bartkovitz, D., Podlaski, F., Janson, C., Tovar, C., Filipovic, Z. M., Higgins, B., Glenn, K., Packman, K., *et al.* (2013) Discovery of RG7388, a potent and selective p53-MDM2 inhibitor in clinical development. *J. Med. Chem.* **56**, 5979–5983

51. Hai, J., Sakashita, S., Allo, G., Ludkovski, O., Ng, C., Shepherd, F. A., and Tsao, M. S. (2015) Inhibiting MDM2-p53 interaction suppresses tumor growth in patient-derived non-small cell lung cancer Xenograft models. *J. Thorac. Oncol.* **10**, 1172–1180

52. Shalem, O., Sanjana, N. E., Hartenian, E., Shi, X., Scott, D. A., Mikkelson, T., Heckl, D., Ebert, B. L., Root, D. E., Doench, J. G., and Zhang, F. (2014) Genome-scale CRISPR-Cas9 knockout screening in human cells. *Science* **343**, 84–87

53. Sanjana, N. E., Shalem, O., and Zhang, F. (2014) Improved vectors and genome-wide libraries for CRISPR screening. *Nat. Methods* **11**, 783–784

54. Schmittgen, T. D., and Livak, K. J. (2008) Analyzing real-time PCR data by the comparative C(T) method. *Nat. Protoc.* **3**, 1101–1108

55. Wang, X., Spandidos, A., Wang, H., and Seed, B. (2012) PrimerBank: A PCR primer database for quantitative gene expression analysis, 2012 update. *Nucleic Acids Res.* **40**, D1144–D1149